## LAMINATED AND SANDWICH PANELS SUBJECT TO BLAST PULSE LOADING

Ugo Icardi and Laura Ferrero

# LAMINATED AND SANDWICH PANELS SUBJECT TO BLAST PULSE LOADING

UGO ICARDI AND LAURA FERRERO

A recently developed optimisation technique is employed for relaxing the interlaminar stress concentration of laminated and sandwich flat panels undergoing impulsive pressure loading. We determine the through-the-thickness distribution of the core properties of sandwich panels and the in-plane distribution of the stiffness properties of their face sheets, as well as that of the constituent layers of laminates maximizing the energy absorbed through wanted modes (e.g., membrane and bending contributions) and minimizing the energy absorbed through unwanted modes (e.g., interlaminar shears). As a structural model, we employ a refined zigzag model with a piecewise high-order variation of in-plane and transverse displacements that fulfils *a priori* the interfacial stress and displacement contact conditions. The zigzag model, a characteristic feature of the method, is incorporated through a strain energy updating into a conventional shear deformable plate element, for the sake of reducing the computational effort required for accurately computing the stresses. The dynamic equations are solved using the Newmark implicit time integration scheme; various pulse pressure time histories are employed. Simple, suboptimal distributions of reinforcement fibres and core density compatible with current manufacturing processes are considered in the numerical applications. It appears that these distributions can effectively reduce the critical interlaminar stress concentration under impulsive loadings, with beneficial effects on the strength at the onset of damage, and improve the dynamic response properties as well.

## 1. Introduction

Pulse pressure loading due to an accidental cause, an explosive device, fuel and nuclear explosions, gust and sonic boom represents for aircraft a major hazard responsible for catastrophic failure of structures. Much research work has been carried out recently in assessing aircraft structures subjected to explosive pressure pulses and for finding configurations able to alleviate their detrimental effects; see [CAA 2001], for example. Although very expensive, full-scale tests of fuselage large sections have been undertaken, showing how the pressure loading hazard could be consistently reduced using hardened luggage containers and sandwich structures. However most of the research is carried out considering panels that are representative of real structural components, often using finite elements for the analysis.

As examples of papers dealing with metallic stiffened panels we mention [Simmons and Schleyer 2006; Rudrapatna et al. 2000; Zhu 1996; Langdon and Schleyer 2006]. Since the structure of modern combat and civil transportation aircraft is often made of or incorporates composite material parts with higher specific strength and stiffness than metals, a growing number of studies have been published about their response to pulse pressure loading. Moreover, new manufacturing techniques render their use economically feasible for large scale applications.

The response of marine sandwich panels to explosion loading has been addressed in [Hayman 1996], [Makinen 1999], [Shin and Geers 1994], [Jiang and Olson 1994] (underwater explosion) and [Houlston et al. 1985] (in air explosion). Studies of the response of aircraft composite panels under impulsive loading include [Cheng and Benveniste 1968; Crocker and Hudson 1969; Rajamani and Prabhakaran 1980; Dobyns 1981; Birman and Bert 1987; Cederbaum et al. 1988; 1989; Librescu and Nosier 1990; Librescu and Na 1998; Song et al. 1998; Librescu et al. 2004; 2006; 2005; Hause and Librescu 2005; 2007; Xue and Hutchinson 2004]. In these studies the blast loads considered were of moderate intensities, so as to not induce damage. The only exception is the last paper, where an elastic-perfectly plastic behaviour was considered. Likewise in other fields, it appears that to realistically describe the dynamic response under impulsive loading, the structural models have to accurately account for the high transverse shear deformation of composites. The present paper, dealing with blast loading of composites, also takes into account the contact conditions at the interfaces of dissimilar constituent materials necessary to keep equilibrium and kinematic compatibility, since many studies have shown their importance for both the overall and the local behaviour.

To account for the interlayer contact conditions and accurately predict the stress fields with an affordable computational effort, we choose as the structural model a refined zigzag model with a piecewise high-order variation of the displacements. The displacement field is postulated in a way that fulfils *a priori* the interfacial stress and displacement contact conditions (namely, continuity of the transverse shear and normal stress components and of displacement), through an appropriate definition of the continuity. The transverse displacement is assumed variable across the thickness, because sandwich composites often fail by crushing, due to the low compressive strength of the core. The model also accounts for internal damage accumulation mechanisms; since composites suffer from microstructures failures while they absorb the incoming energy, they can fail in service at load levels much lower than the ultimate design load. The model has been successfully applied to impact studies of laminated [Icardi 2007] and sandwich [Icardi and Ferrero 2009] flat panels, where it efficiently predicted the impact induced damage, as shown by comparisons with the damage detected by ultrasonic cartography, and to the stress analysis of thick damaged sandwich panels, as shown by comparisons with the exact elasticity solution [Icardi and Ferrero 2009].

To lower the cost of the analysis, both this paper and in the works just mentioned, the zigzag model is incorporated into a standard eight-node plate element based on first-order shear deformation plate theory (FSDPT) through an energy updating procedure that is locally carried out in the post-processing phase.

A recently developed optimisation technique [Icardi and Ferrero 2008] is employed for finding the appropriate spatial distribution of the stiffness properties (fibers orientation and core density) that minimize the out-of-plane stresses due to impulsive loading. It is found solving the Euler–Lagrange equations of an optimisation problem in which the absorbed energy due to out-of-plane stresses is minimised, while that due to membrane stresses is maximised. As a preparatory step to the response analysis, the structural model and the optimisation technique will be briefly discussed.

## 2. Structural model

As mentioned, the present structural model uses a conventional plate element for a preliminary analysis and locally improves its predictive capability by updating its strain energy to that of a zigzag model with

a piecewise cubic variation of the membrane displacements across the thickness and a fourth-order variation of the transverse displacement. The merit of the zigzag model is to provide accurate results with low computational effort, since the interfacial stress and displacement contact conditions are fulfilled *a priori* and not as constraints that increase the number of the governing equations. Its drawback is the involvement of displacement derivatives as nodal degrees of freedom, which prevents a direct implementation into a finite element. To overcome this problem, we use the updating process of [Icardi 2007; Icardi and Ferrero 2009] with some improvements (outlined below) and the same failure and post-failure models.

### 2.1. *Kinematics of the zigzag model.*

Assume the laminated or sandwich panel to consist of $S$ layers of different thickness and material properties, the core being treated as a thick layer in a multilayer construction. The accuracy of this hypothesis have been extensively assessed in a number of previous papers, even in the case of a thick, damaged sandwich panel as previously mentioned .

As reference system use a Cartesian coordinate system $(x, y, z)$, with $(x, y)$ on the reference midplane and $z$ as the thickness coordinate. Indicate with $U$, $V$ the in-plane and $W$ the out-of-plane displacement components and with $\sigma_{xz}$, $\sigma_{yz}$ and $\sigma_{zz}$ the out-of-plane stresses. Use a subscript comma to indicate differentiation. The displacement field is represented as

$$
\begin{aligned}
U(x, y, z) &= u(x, y, z) + \mathsf{U}(x, y, z), \\
V(x, y, z) &= v(x, y, z) + \mathsf{V}(x, y, z), \\
W(x, y, z) &= f_w^1(x, y, z) + f_w^2(x, y, z).
\end{aligned}
\tag{1}
$$

That is, the in-plane components are expressed as sums of contributions $u$, $v$ that are continuous and have continuous first derivatives across the thickness, as in the equivalent single layer models

$$
\begin{aligned}
u(x, y, z) &= u^\circ + z(\gamma_x^\circ - w_{,x}^\circ) + z^2 C_x(x, y) + z^3 D_x(x, y), \\
v(x, y, z) &= v^\circ + z(\gamma_y^\circ - w_{,y}^\circ) + z^2 C_y(x, y) + z^3 D_y(x, y).
\end{aligned}
\tag{2}
$$

and contributions $\mathsf{U}$ and $\mathsf{V}$ that are continuous but have discontinuous first derivatives at the interfaces:

$$
U(x, y, z) = \sum_{k=1}^{S-1} {}^{(k)}\phi_x(x, y)(z - {}^{(k)}Z^+)H_k, \quad V(x, y, z) = \sum_{k=1}^{S-1} {}^{(k)}\phi_y(x, y)(z - {}^{(k)}Z^+)H_k.
\tag{3}
$$

The transverse displacement is the sum of a contribution

$$
f_w^1(x, y, z) = a(x, y),
\tag{4}
$$

representing the displacement of the reference midplane $w^\circ$, and a field with discontinuous derivatives at the interfaces,

$$
\begin{aligned}
f_w^2(x, y, z) = {}&zb(x, y) + z^2 c(x, y) + z^3 d(x, y) + z^4 e(x, y) \\
&+ \sum_{k=1}^{S-1} {}^{(k)}\psi_x(x, y)(z - {}^{(k)}Z^+)H_k \sum_{k=1}^{S-1} {}^{(k)}\psi_y(x, y)(z - {}^{(k)}Z^+)^2 H.
\end{aligned}
\tag{5}
$$

The piecewise continuous contributions to the displacements, namely (3) and (5), are expressed in terms of functions ${}^{(k)}\Phi_x$, ${}^{(k)}\Phi_y$, ${}^{(k)}\Psi_1$, ${}^{(k)}\Psi_2$, which we call continuity functions, and which are determined by enforcing the continuity of the transverse shear and normal stresses $\sigma_{xz}$, $\sigma_{yz}$, $\sigma_{zz}$ and of the gradient $\sigma_{zz,z}$

at the interfaces, as prescribed by elasticity theory. Since the Heaviside unit step function $H_{.k}$ appearing in the previous equations is defined only in $\mathbb{R}^+$, the continuity functions are computed starting from the bottom layer, the choice of the starting layer as the upper- or lowermost being immaterial.

The remaining functions $C_x$, $C_y$, $D_x$, $D_y$, $b$, $c$, $d$, $e$ are determined enforcing the fulfilment of the boundary conditions at the upper $^{(u)}$ and lower $^{(l)}$ bounding faces, namely the stress-free boundary conditions on the transverse shears and the conditions

$$\sigma_{zz}^u = p_o^u, \quad \sigma_{zz}^l = p_o^l, \quad \sigma_{zz,z}^u = \sigma_{zz,z}^l = 0$$

on the transverse normal stress. The symbols $p_o^u$, $p_o^l$ represent the transverse distributed loading at the upper and lower bounding faces, respectively.

As mentioned, this model will be implemented operating an updating of the nodal degree of freedoms (DOFs) of a FSDPT parent element through an energy updating process in the post-processing phase. This updating process avoids a direct implementation of the zigzag model, which turns out to be inefficient by the computational viewpoint, because derivatives should appear in the vector of nodal DOFs that are consequent to the enforcement of the stress continuity conditions.

The updating is carried out through corrective terms that in the present paper are determined in closed form using a symbolic calculus tool. This technique will be outlined in the following Section. No details will be given about the eight node FSDPT parent element because it has standard features; the reader finds the omitted details in [Icardi 2007].

Note that since the functional degrees of freedom of this model $u^{(o)}$, $v^{(o)}$, $w^{(o)}$, $\gamma_x$ and $\gamma_y$ coincide with those of the FSDPT model, it is possible to update the strain energy of such a lower order model to that of the current zigzag model, with the purpose and by the technique described hereafter. Also note that the FSDPT and the HSDPT models can be particularized from the zigzag model neglecting the contributions (3) and (5) and, in the case of the FSDPT model, considering only the linear case (2).

A finite element approach is chosen in order to easily treat the spatially variable material properties that result from the tailoring optimization process, and in order to enable the analysis of a spatially variable pressure pulse loading such as the NOL pressure model profile [Proctor 1972], that will be the object of a future application.

### 2.2. *Energy updating and post-processing.*  As is well known, any model that cannot be refined across the thickness, like the present one, needs integration of the local equilibrium differential equations

$$
\begin{aligned}
(*\sigma_{xz} - \underline{\sigma_{xz}}) &= -(\langle \underline{\sigma_{xx,x}} + \underline{\sigma_{xy,y}} \rangle + \underline{\sigma_{xz}}), \\
(*\sigma_{yz} - \underline{\sigma_{yz}}) &= -(\langle \underline{\sigma_{xy,x}} + \underline{\sigma_{yy,y}} \rangle + \underline{\sigma_{yz}}), \\
(*\sigma_{zz} - \underline{\sigma_{zz}}) &= -(\langle *\sigma_{xz,x} + *\sigma_{yz,y} \rangle + \underline{\sigma_{zz}})
\end{aligned}
\tag{6}
$$

to provide a realistic description of the interlaminar stress fields (in the former equations the underlined stresses are those computed from the constitutive equations). To make integration computationally efficient and preserve accuracy, we adopt two procedures in this paper:

 (i) The strain energy of the FSDPT eight-node elements is updated to that of the zigzag model.

 (ii) The results by the FSDPT elements are interpolated and smoothed with spline functions in the region where the stress analysis is carried out.

The goal is to derive these interpolations instead of the shape functions, because the interpolated quantities have a higher-order representation and thus they do not lose accuracy. So, although standard, efficient parabolic shape functions are used in the finite element model, no accuracy is lost integrating the local differential equilibrium equations.

It is remarked that the post-processing operations are much more cost-effective than using discrete-layer models with a large number of DOFs, because they are carried out only locally and their convergence is fast. The present approach achieves the accuracy of closed-form approaches with a low computational effort, but it is more versatile, because it allows complex geometry, loading, boundary conditions and a point-to-point material property variation to be treated. Note that the updating procedure prevents the locking effects, since the transverse displacement and the shear rotations are described with their right interdependence; see Equations (7) immediately below.

**2.2.1.** *Computation of the continuity constants.* The first operation is the computation of the constants appearing in the continuity functions. The readers are referred to [Icardi 2001] for a detailed discussion of these functions, whose purpose is to ensure the fulfilment of the interfacial contact conditions. To make this operation more efficient than in the former versions of the software, here a symbolic calculus tool is employed to provide expressions in closed form. The DOFs of the FSDPT must be rearranged in order to be consistent with the representation of the zigzag model:

$$\theta_x = z(\gamma_x^\circ - w_{,x}^\circ), \qquad \theta_y = z(\gamma_y^\circ - w_{,y}^\circ). \tag{7}$$

Assume $u^{(o)}$, $v^{(o)}$, $w^{(o)}$, $\gamma_x$ and $\gamma_y$ are the functional DOFs of the FSDPT model; the homologous terms with a tilde ~ be those of the zigzag model, are obtained from the earlier ones adding unknown corrective terms:

$$\tilde{u}^\circ = \hat{u}^\circ + \Delta\hat{u}^\circ, \quad \tilde{v}^\circ = \hat{v}^\circ + \Delta\hat{v}^\circ, \quad \tilde{w}^\circ = \hat{w}^\circ + \Delta\hat{w}^\circ,$$
$$\tilde{\gamma}_x^\circ = \hat{\gamma}_x^\circ + \Delta\hat{\gamma}_x^\circ, \quad \tilde{\gamma}_y^\circ = \hat{\gamma}_y^\circ + \Delta\hat{\gamma}_y^\circ. \tag{8}$$

In the current version of the software is no longer necessary to start with $f_w^2 = 0$ and then make them consistent in a subsequent step. The continuity functions computed in this way are those corresponding to the DOFs provided by the preliminary calculus using the FSDPT finite elements. The result of this calculus will be improved by the following operations.

**2.2.2.** *Updating of the energy due to transverse shears.* This operation is performed equating again the homologous quantities of the FSDPT and zigzag models, using the representation of Equations (8):

$$(\boldsymbol{q}_e + \Delta\boldsymbol{q}_{eK})^T \boldsymbol{K}_{fsdpt}(\boldsymbol{q}_e + \Delta\boldsymbol{q}_{eK}) = \boldsymbol{q}_e^T \boldsymbol{K}_{zigzag}\boldsymbol{q}_e. \tag{9}$$

The symbol $\boldsymbol{q}_e$ represents the vector of nodal DOFs; $\Delta\boldsymbol{q}_{eK}$ are the corrective terms; $\boldsymbol{K}$ is the stiffness matrix (only the rows and columns relative to the out-of-plane shears). The left hand size member is based on the FEM model, while the right hand side is an analytic expression. The solution is found in closed form via symbolic calculus assuming as unknown only the transverse shear rotations. Subsequently, the other DOFs are updated one at a time, reiterating the entire process till convergence.

**2.2.3.** *Transverse normal stress and strain.* Since this contribution that plays a primary role for sandwich panels is disregarded in the FSDPT parent element, it is approximated at a local point in the post-processing phase. This operation is carried out integrating the third local differential equilibrium

equation, where a spline interpolation of the previously computed transverse shear stresses is used. Then an approximate expression of the transverse normal strain $^o\varepsilon_{zz}$ is obtained by the stress–strain relation of elasticity

$$^0\varepsilon_{zz} = \sigma_{xx}S_{13} + \sigma_{yy}S_{23} + {}^0\sigma_{zz}S_{33} + \sigma_{yz}S_{34} + \sigma_{xz}S_{35} + \sigma_{xy}S_{36}. \tag{10}$$

Using these approximated transverse normal stress and strain, their contribution to the strain energy is computed. In the current version, the energy balance is used to compute improved transverse shear stress rotations and the variation of the out-of-plane displacement across the thickness in closed form, in combination with the local differential equilibrium equations. Once the improved stresses have been computed, they are interpolated with spline functions for the subsequent operations. This process is restarted with the improved transverse shear and transverse displacement DOFs and repeated till convergence.

**2.2.4.** *Updating of the membrane energy.* The displacements and stresses computed at this stage are used for improving the membrane energy and thus for computing refined in-plane DOFs. To this purpose, the in-plane displacements are represented as in $(8)_{1,2}$ and the strain energy as in Equation (9), where only the rows and columns relative to the membrane energy contributions are retained. The solution is found substituting the corrected displacements one at a time and reiterating the entire process till convergence.

**2.2.5.** *Updating of the work of inertial forces.* The expression of the work of inertial forces is used to make the dynamics of the FSDPT model with that of the zigzag model:

$$(\boldsymbol{q}_e + \Delta\boldsymbol{q}_{eM})^T \boldsymbol{M}_{\text{fsdpt}}(\boldsymbol{q}_e + \Delta\boldsymbol{q}_{eM})^T F_f(t) = \boldsymbol{q}_e{}^T \boldsymbol{M}_{\text{zigzag}}\boldsymbol{q}_e{}^T F_{zz}(t). \tag{11}$$

$\boldsymbol{M}_{\text{fsdpt}}$ and $\boldsymbol{M}_{\text{zigzag}}$ being their consistent mass matrices, $\boldsymbol{q}_e$ the converged vector of nodal DOFs after the steps up to 2.2.4, and $\Delta\boldsymbol{q}_{eM}$ the corrective terms. Since the previous equation must hold irrespective of the time evolution of the solution, it can be rearranged as:

$$(\boldsymbol{q}_e + \Delta\boldsymbol{q}_{eM})^T \boldsymbol{M}_{\text{fsdpt}}(\boldsymbol{q}_e + \Delta\boldsymbol{q}_{eM})^T = \boldsymbol{q}_e{}^T \boldsymbol{M}_{\text{zigzag}}\boldsymbol{q}_e{}^T. \tag{12}$$

The corrective terms are computed in closed form at each iteration one at a time and reiterating till convergence. The sequence of steps 2.2.1–2.2.5 is repeated till convergence, using the current stresses and displacements at the end of each iteration as entry values for the subsequent one. The convergence of the energy updating procedure appeared fast whenever applied. The energy updating appeared always able to consistently improve the quality of the stress predictions and did not heavily affect the overall computational costs.

**2.3.** *Failure and progressive damage accumulation.* The present structural model incorporates criteria for matrix cracking, fibres failure, delamination and core crushing in order to account for all the possible failure modes and their reciprocal interactions. Only macromechanical, stress-based criteria using standard, easy to assess, engineering properties are here employed, since they are the only ones with an affordable computational effort for the transient analysis. The formulation is that successfully adopted in [Icardi 2007; Icardi and Ferrero 2009]. A 3D version of the Hashin's criterion with in situ strengths is used to predict the failure of fibres and matrix. For the tensile failure of fibres we have

$$\left(\frac{\sigma_{11}}{X^t}\right)^2 + \frac{1}{S_{12=13}{}^2}(\tau_{12}{}^2 + \tau_{13}{}^2) = 1 \quad (\sigma_{11} > 0) \tag{13}$$

while for compressive failure we have

$$\sigma_{11} = -X^c \quad (\sigma_{11} < 0).$$

The expression for the matrix failure under traction is

$$\left(\frac{\sigma_{22} + \sigma_{33}}{Y^t}\right)^2 + \frac{1}{S_{23}{}^2}(\tau_{23}{}^2 - \sigma_{22}\sigma_{33}) + \left(\frac{\tau_{12}}{S_{12=13}}\right)^2 + \left(\frac{\tau_{13}}{S_{12=13}}\right)^2 = 1 \quad (\sigma_{22} + \sigma_{33} > 0),$$

while for compressive failure it is

$$\frac{1}{Y^c}\left(\left(\frac{Y^c}{2S_{23}}\right)^2 - 1\right)(\sigma_{22} + \sigma_{33}) + \frac{1}{4S_{23}{}^2}(\sigma_{22} + \sigma_{33})^2 + \frac{1}{S_{23}{}^2}(\tau_{23}{}^2 - \sigma_{22}\sigma_{33}) + \frac{1}{S_{12=13}{}^2}(\tau_{12}{}^2 + \tau_{13}{}^2) = 1$$

$$(\sigma_{22} + \sigma_{33} < 0).$$

To compare the same failures with a different formulation, the criterion of Hou et al. is incorporated into the structural model, which predicts the failure of fibres by the formula

$$\left(\frac{\sigma_{11}}{X^t}\right)^2 + \left(\frac{\tau_{12} + \tau_{13}}{S_f}\right)^2 = 1$$

and the tensile and compressive failures of the matrix, respectively, by

$$\left(\frac{\sigma_{22}}{Y^t}\right)^2 + \left(\frac{\tau_{12}}{S_{12}}\right)^2 + \left(\frac{\tau_{23}}{S_{m23}}\right)^2 = 1, \qquad \frac{1}{4}\left(\frac{-\sigma_{22}}{S_{12}}\right)^2 + \frac{(Y^c)^2\sigma_{22}}{4S_{12}^2 Y^c} - \frac{\sigma_{22}}{Y^c} + \left(\frac{\sigma_{12}}{S_{12}}\right)^2 = 1.$$

This criterion is also used to predict the onset of delamination, together with the Chang–Springer criterion. The criterion of Hou et al. predicts delamination by the expressions

$$\left(\frac{\sigma_{33}}{Z_T}\right)^2 + \frac{(\tau_{12}{}^2 + \tau_{13}{}^2)}{S_{13}{}^2(d_{ms}d_{fs} + \delta)} = 1 \quad (\sigma_{33} \geq 0),$$

$$\frac{(\tau_{12}{}^2 + \tau_{13}{}^2 - 8\sigma_{33}{}^2)}{S_{13}{}^2(d_{ms}d_{fs} + \delta)} = 1 \quad \left(-\sqrt{\tfrac{1}{8}(\sigma_{13}^2 + \sigma_{23}^2)} \leq \sigma_{33} < 0\right),$$

while the Chang–Springer criterion uses the expression

$$\left(\frac{\sigma_{33}}{Y^t}\right)^2 + \left(\frac{\tau_{13}}{S_{13=23}}\right)^2 + \left(\frac{\tau_{23}}{S_{13=23}}\right)^2 = 1.$$

To predict the sandwich core failure in crushing mode, we use the criterion by Besant et al.,

$$\left(\frac{\sigma_{zz}}{\sigma_{cu}}\right)^n + \left(\frac{\tau_{xz}}{\tau_{lu}}\right)^n + \left(\frac{\tau_{yz}}{\tau_{lu}}\right)^n = e_{\text{core}},$$

where $\sigma_{cu}$ and $\tau_{lu}$ being the core strengths in compression and transverse shear; it predicts failure of the core when $e_{\text{core}} > 1$.

The exponent $n = 1.5$ is assumed, since it best fits the experimental results. In the event of crushing, the work done by the inner crush force has to be accounted for; therefore the through-the-thickness variation of the transverse displacement by the updating subprocedure of Section 2.2.3 has to be considered.

The degradation of the properties after failure is simulated using the ply-discount theory. Namely, the elastic moduli in the subelement regions where the spline interpolation is performed are locally degraded according to the rule

$$Q_{\text{after}} = Q_{\text{before}} 10^{-m} \qquad \text{with } 0 \le m \le 20,$$

$Q_{\text{after}}$ and $Q_{\text{before}}$ being Young's and shear elastic moduli selected according to the type of failure occurred. This implies that within the time steps, the stiffness coefficients have to be locally reduced in the region where the damage arose and the stiffness properties locally modified during the process, choosing an appropriate exponent $m$. In event of fibre failure, $E_{11}$, $G_{12}$, and $\nu_{12}$ are reduced, while for matrix failure $E_{22}$, $G_{12}$, and $\nu_{12}$ are reduced. In the event of delamination, $G_{13}$ and $G_{23}$ are reduced. More complex degradation models in a better harmony with the physics are not considered, their effort being too large.

Nevertheless a failure model is implemented with the features outlined above, in the numerical applications the pulse pressure loading will be of a moderate intensity that will not induce damage, so the analysis of the effects of an intense loading is left to a future study.

## 3. Blast pulse modelling

When a pressure pulse is generated, a shock wave is transmitted in all directions. Once this wave reaches a structure, it produces an instantaneous pressure peak, followed by a decrease. Various expressions have been proposed for describing the overpressure time history, either of theoretical or numerical nature. Also results of experiments have been published in the literature.

Since most of the studies are analytical or based on a finite element analysis, usually an analytical overpressure time history is adopted. Customary the blast-type loading is described in terms of the modified Friedlander exponential decay equation[1]

$$P_z(t) = P_m(1 - t/t_p)e^{-a't/tp}, \tag{14}$$

$P_m$ being the peak pressure in excess of the ambient one, $t_p$ the positive phase duration measured from the time of arrival of the blast and $a'a$ decay parameter that can be adjusted in order to approximate the result of an experimental test. Customarily the pressure is assumed to be uniformly distributed over the entire panel and the impact is assumed to occur with a normal incidence having in view the large dimension of the blast front. This is not the case of gun blast pressure pulses, which require the spatial distribution of the pressure pulse to be considered; the readers find a recent study about gun blast in the paper by [Kim and Han 2006].

Assuming $a'/t_p$ equal to zero, the limiting case of the triangular loading is featured. As other special cases, the rectangular, step and sine pressure pulses have been considered in literature.

The sonic boom-type loading is customary modelled as an $N$-shaped pressure pulse corresponding to an idealized far-field pulse impacting at a normal incidence:

$$P_z(t) = \begin{cases} P_m(1 - t/t_p) & \text{for } 0 < t < rt_p, \\ 0 & \text{for } t < 0 \text{ and } t > rt_p, \end{cases} \tag{15}$$

---

[1]See the pioneering papers [Gupta 1985; Gupta et al. 1986] and applications in [Cederbaum et al. 1988; 1989; Librescu and Nosier 1990; Librescu and Na 1998; Song et al. 1998; Librescu et al. 2004; 2006; 2005; Hause and Librescu 2005].

where $r$ denotes the shock pulse length factor and the other symbols are as in (14). For the case $r = 1$, the $N$-shaped pulse degenerates into a triangular distribution, while for $r = 2$ a symmetric pulse is obtained.

The former pulse pressure time histories of (14) and (15) have been incorporated in the impact computational model of [Icardi 2007] at the place of the contact force time history. However any other analytical or computational model could be used.

The dynamic response problem resulting from blast pulse pressure loading $M\ddot{q}_e + C\dot{q}_e + Kq_e = F$, where $M$, $C$ and $K$ denote the mass, damping and stiffness matrices, respectively, while $q_e$ is the vector of nodal DOFs and $F$ is the vector of the nodal forces, is solved using the Newmark implicit time integration scheme, because this technique, at the contrary of explicit schemes, is stable for reasonably large time steps.

In the present numerical applications only the undamped motions will be considered; work is in progress in order to account for damping, which has implications on the thermodynamic constraints involved in the tailoring optimization process.

## 4. Tuning of the energy absorption properties

In this paper, a technique for tuning the energy absorption properties of laminated and sandwich composites is presented, which is based on a new tailoring concept. The purpose is to minimize the energy absorbed through unwanted modes (those involving interlaminar strengths) and maximize the energy absorbed through desired modes (those involving membrane strengths). This is done by finding a suited variable distribution of stiffness properties, an extension of the one developed by the authors in [Icardi and Ferrero 2008]. While this former version only dealt with an in-plane variation of properties of laminates, in the current version either a variation of the stiffness properties of the face sheets over their plane, or of the core properties across the thickness of sandwich composites are considered.

The suitable distribution of stiffness properties is obtained solving the Euler–Lagrange equations of a problem where the strain energy contributions of interest are made extremal under spatial variation of such properties.

The effect of this technique is to act as an energy absorption tuning, since the amount of energy absorbed by specific modes can be minimized or maximized. Minimization of the energy due to out-of-plane strains and stresses can result in a reduction of these very critical parameters by the viewpoint of damage accumulation in service, as shown by the numerical applications. This result can be obtained without any stiffness loss, since the membrane and bending energy contributions can be maximized, while the energy of out-of-plane stresses is minimized.

The present technique can be seen as a non classical optimization technique in which the design variables to be modified are the stiffness properties (through spatial variation of the ply angles and/or of fibre volume fraction and constituent materials) and the constraints are represented by imposition of constant thickness of individual layers, constant overall properties (e.g. averaged stiffness of the "optimized" layers equal to the stiffness of classical layers made of the same constituent materials), the thermodynamic constraints for energy conservation and the Lempriere, Lekhnitski and Chentsov's conditions. The objective function is the extremization of wanted energy contributions of interest, while the optimization algorithm can be seen as the variational calculus rule, i.e. imposition of the first variation vanishing.

Note that in the applications, pre-existing conventional layers will be substituted with layers that either (i) minimizes bending and maximizes membrane energy, (ii) minimizes bending and maximizes transverse shear, or (iii) maximizes bending and minimizes transverse shear, because for each of these three cases a solution was found in [Icardi and Ferrero 2008] that does not make contradictory these requirements.

The following simplified version of the structural model with a constant transverse displacement is employed in this context:

$$U(x, y, z) = u^\circ + z(\gamma_x^\circ - w_{,x}^\circ) + z^2 C_x(x, y) + z^3 D_x(x, y) + \sum_{k=1}^{S-1} {}^{(k)}\phi_x(x, y)(z - {}^{(k)}Z^+)H,$$

$$V(x, y, z) = v^\circ + z(\gamma_y^\circ - w_{,y}^\circ) + z^2 C_y(x, y) + z^3 D_y(x, y) + \sum_{k=1}^{S-1} {}^{(k)}\phi_y(x, y)(z - {}^{(k)}Z^+)H_k, \quad (16)$$

$$W(x, y, z) = w^\circ,$$

since the model of (1)–(5) requires too big a mathematical effort. Higher-order contributions neglected in the simplification will be accounted for by updating its strain energy to that of the model (1)–(5).

**4.1.** *Tailoring of constituent plies.* This optimisation is carried out finding spatially variable stiffness properties which makes the bending, in-plane and out-of-plane strain energy contributions stationary, with the purpose to minimise the energy absorbed by modes involving out-of-plane stresses and strains and maximise that related to membrane stresses and strains. The stiffness properties of the constituent layers (i.e., the face sheets in the case of sandwich panels) represent the master field, while the other variables not subjected to variation represent the slave and data fields. The optimisation starts writing the first variation of the strain energy under variation of the functional DOFs that represents the constraint of dynamic equilibrium.

A rather intricate system of coupled partial differential equations are obtained, the so-called Euler–Lagrange equations and related natural boundary conditions, enforcing the vanishing of the first variation of the strain energy under variation of the stiffness properties, that define the optimised distributions of these properties (i.e., that make the considered energy contributions extremal). We report as an example the stationary condition for the bending energy:

$$-WR_1\delta u^\circ - WR_2\delta v^\circ - WR_3\delta w^\circ + (WR_4 - \tfrac{4}{3}WR_5 + WR_6 + WR_7)\delta\gamma_x^\circ$$
$$+ (WR_8 - \tfrac{4}{3}WR_9 + WR_{10} + WR_{11})\delta\gamma_y^\circ = 0, \quad (17)$$

where the *WR*'s are sums of partial derivatives of various orders of the stiffness quantities; for instance

$$WR_3 = D_{11,1111} + 2D_{12,1122} + 4D_{16,1112} + 4D_{26,1222} + 4D_{66,1122} + D_{22,2222}. \quad (18)$$

Similarly, the expression for the transverse shear energy in the plane $(x, z)$ is a sum of multiples of $\delta u^\circ$, $\delta v^\circ$, $\delta w^\circ$, $\delta\gamma_x^\circ$ and $\delta\gamma_y^\circ$; the coefficient of the first of these is one of the simplest and will serve to give the flavor:

$$\Big\{ XR_{R1} + XR_{R1}^a + XR_{R1}^d + XR_{R44} + XR_{R44}^a + XR_{S44}^d - \tfrac{4}{3}(XR_{P1} - XR_{P6})/h^2$$
$$- \tfrac{1}{2}(XR_{26X2} + XR_{31X2} + XR_{36X2} + XR_{41X2})/h - \tfrac{2}{3}(XR_{26X3} + XR_{31X3} + XR_{36X3} + XR_{41X3})/h^2 \Big\}\delta u^\circ.$$

(The *XR* are also defined in terms of partial derivatives of the stiffness quantities.)

At this point, we must add to the system of governing equations also the constraint conditions representing the energy updating from the simplified model of (16) to that of the model of (1) with variable transverse displacement. An approximate solution of technical interest to this governing system of equations is a second-order polynomial approximation of the transformed reduced stiffness coefficients distribution, since it can be easily obtained by current manufacturing techniques:

$$
\begin{aligned}
&Q_{11} = A_1 + A_2 x + A_3 x^2, && Q_{12} = C_1 + C_2 x + C_3 y + C_4 x^2 + C_5 y^2 + C_6 xy, \\
&Q_{16} = E_1 + E_2 x + E_3 x^2 + E_4 xy, && Q_{22} = B_1 + B_2 y + B_3 y^2, \\
&Q_{26} = F_1 + F_2 y + F_3 y^2 + F_4 xy, && Q_{44} = G, \qquad Q_{55} = L, \\
&Q_{45} = M, && Q_{66} = D_1 + D_2 x + D_3 y + D_4 x^2 + D_5 y^2 + D_6 xy.
\end{aligned}
\tag{19}
$$

This approximation holds at the laminate level (i.e., for a group of layers that together makes extremal the energy contributions of interest), or at the single ply level (i.e., of a layer able itself to minimise or maximise certain energy contributions).

The quantities $A_1$, $A_2$, ..., $B_1$, ..., $F_1$, ..., $M$ appearing in (19) are determined by enforcing conditions that make the solution physically consistent. The thermodynamic constraints, the conservation of energy and the conditions formulated by Lempriere, Lekhnitski and Chentsov's are enforced in this paper. In addition, a mean value of the stiffness coefficients is imposed; it is assumed equal to that of the conventional layers that are replaced with the optimised ones. Also a convex or a concave shape can be chosen, together with the value of the stiffness at the bounds of the region. The coefficients of $Q_{12}$ and $Q_{66}$ are determined enforcing the mean value and the thermodynamic constraints. $Q_{16}$, $Q_{26}$ are enforced to have a zero mean value, while the coefficients of $Q_{44}$, $Q_{45}$ and $Q_{55}$ are determined enforcing Chentsov's relations.

We remark that the variable distribution of stiffness properties, (19), can be obtained either varying the orientation of the reinforcement fibres, the fibre volume rate or the constituent materials (i.e. fibres and matrix) over the plane of the plies. It is also remarked that as shown in [Icardi and Ferrero 2008], even a rough approximation of the elastic coefficients of (19) using patches with a step variation of the orientation can be effective.

### 4.2. *Core with variable properties.*

The stiffness discontinuity at the face sheet/core interface results in a large increase in interfacial shear stresses, so debonding at or near the core/face sheet interface is a major problem in sandwich construction. An alternative for overcoming this problem is a sandwich structure with a functionally graded core: grading the core properties in the thickness direction allows a reduction in the stiffness discontinuity. Although their technology is still in its infancy, functionally graded materials are of great interest for their potential in many applications. New fabrication methods are expected to be developed in the next years that will control the foaming process parameters as required [Apetre et al. 2006]. For such reason, the advantages of these new sandwich structures are here assessed. Assuming that the core properties can be controlled across the thickness, the strain energy due to transverse stresses and strains have to be made extremal for finding core property distributions that reduce the interlaminar stress concentration at the face sheet/core interfaces. As an example we report the extremal condition for the energy due to the shear in the plane $(x, z)$:

$$\int \Big( Q_{11}(z^2 G^y_{,x} - z^2 W^y_{,xx} + zU^y_{,x}) + Q_{12}(zV - z^2 W_{,y} + z^2 H)$$

$$+ Q_{16}(2zU + 2z^2 G - 3z^2 W_{,x} - zV^y_{,x} + z^2 H^y_{,x}) + Q_{26}(zV^x_{,y} - z^2 W_{,yy} + z^2 H^x_{,y})$$

$$+ Q_{66}(zV + zU^x_{,y} - 2z^2 W_{,y} + z^2 H + z^2 G^x_{,y}) + Q_{44}G^{xy} + Q_{45}H^{xy}\Big) dz. \quad (20)$$

We give some of the expressions for the symbols appearing in this equation, as examples:

$$\int u^0_{,x}dx = U, \quad \int v^0_{,x}dx = V, \quad \int w^0_{,x}dx = W, \quad \int \gamma_{x,x}dx = G, \quad \int \gamma_{y,x}dx = H,$$

$$\int U \, dy = U^y, \quad \int V \, dy = V^y, \quad \int W \, dy = W^y, \quad \int G \, dy = G^y, \quad \int H \, dy = H^y.$$

The terms not reported here also contain derivatives of the DOFs integrated over the domain. As in the former case of the optimisation of face sheets, one must add the constraints representing the equilibrium and the updating from the simplified model of (16) to the model of (1). As a final result, the following condition is obtained, that defines the core properties distribution that makes the energy of transverse shears extremal:

$$\int Q_{ij}(z)F \, dz = \text{constant}, \quad (21)$$

where $F = A + Bz$, with $A$ and $B$ representing integrals of the spatial derivatives of the displacements in $(x, y)$. Similar considerations hold for the membrane energy contributions. In this case, the extremal conditions correspond to

$$F = Az^2 + Bz. \quad (22)$$

This equation holds for the elastic coefficients $Q_{11}$, $Q_{12}$, $Q_{22}$, $Q_{16}$, $Q_{26}$ and $Q_{66}$, while in the case of $Q_{44}$, $Q_{45}$ and $Q_{55}$, the quantity $F$ has to be set equal to 1. Accordingly, the stiffness properties $Q_{11}$ to $Q_{66}$ have to vary across the thickness according to $(Az^2 + Bz)^{-1}$, while $Q_{44}$, $Q_{45}$ and $Q_{55}$ have to be constant.

If we assume the foam constituting the core to be an isotropic material with properties $E$, $G$ and $\upsilon$ and represent its stiffness coefficients as $Q_{11} = K_1/(z^2 + C_1 z)$, $Q_{12} = K_2/(z^2 + C_2 z)$, we find the following relation after enforcement of thermodynamic and isotropy constraints:

$$-2K_1 < K_2 < K_1. \quad (23)$$

In the numerical applications, the properties of the core will be assumed to vary according to the former relations (19) to (23) considering as upper and lower limits those of the ROHACELL foam.

## 5. Numerical results

The accuracy of the present structural model with energy updating was extensively assessed in a number of previously published papers. The reader is referred, among other recent papers by the authors not cited for brevity, to [Icardi 2007] for laminates and to [Icardi and Ferrero 2009] for sandwich plates with or without damage. In all these assessments, the result of the simulation in terms of stress fields, damage and impact force time history were compared to the exact 3D elasticity solution, where available, and to experiments. The model always appeared accurate with a low computational effort (less that two minutes

on a PC with a 1.9 GHz dual core processor); therefore no further assessments will be presented in this paper.

Our purpose is to test whether the optimisation of layers and core can relax the critical interlaminar stress concentrations and then improve the strength at the onset of delamination (without any loss of bending stiffness or decay of the response properties).

As a necessary premise, comparisons by the results of the present simulation to the results by Librescu and co-workers will be presented for sample cases taken from [Librescu and Nosier 1990; Hause and Librescu 2005], with the purpose to assess whether the higher-order effects by the present model (necessary for capturing the 3D stress fields) improve the accuracy of the dynamic response. To this purpose, also the results of a closed-form approach based on the model of Section 2.1 and solution of the governing equations by the Galerkin method will be presented for comparisons. The reader can find details in [Icardi 2007], where this approach was used for computing the contact force time history. Note that while in the impact study of [Icardi 2007] up to 15 terms were required to represent the waves that reach the edges and reflect off during the contact time, in the current case no change in the results was seen up to 11 terms. Since the FSDPT model can be particularised from the zigzag model of (1)–(5), the response of this model will also be used for comparisons.

It will be shown that the results by Librescu and co-workers agree with those obtained by the FSDPT model using a single term, while using more terms high-order effects will be evidenced as little larger deflections and lower frequencies. This behaviour is believed to be correct, since the improved description of the shear deformation and the inclusion of the energy associated to the transverse normal stress and strain modes make the structural model a little less stiff.

Hereafter results will be presented for laminated and sandwich panels with laminated faces under blast loading. Note that sandwich composites represent much more severe test cases from the viewpoint of modelling, since they require a refined modelling that accounts for large transverse shear and normal deformations.

**5.1.** *Laminated plates.* Consider a pinned [0/90/90/0] laminated square plate with a length-to-thickness ratio of 30, undergoing a pressure pulse characterised by $a'/t_p = 0$ in (14), $P_m = 3.447$ MPa and $t_p = 0.1$ s, according to [Librescu and Nosier 1990, Figure 3], which is here referred as the classical case. The deflection will be presented for all the studied cases in a non-dimensional form, as the ratio between the dynamic displacement and the static one. The non-dimensional deflection predicted by the present finite element model with energy updating (in-plane discretization into $10 \times 10$ elements) is represented in Figure 1, left, where it is compared with the predictions of the closed-form approach based on the Galerkin's method for 11 terms in both $x$ and $y$ directions, as predicted by the zigzag model of Section 2.1 and by the CLPT (classical laminated plate theory) and FSDPT models with only one term in both directions. Figure 1, right, shows the response when the effects of damage are assessed while time unfolds.

According to [Librescu and Nosier 1990], the normalisation of results is carried out with respect to the deflection of the static case. In the damaged case, this reference deflection is computed when the delaminated area at the most critical interface (the one next to the impacted face) is 50%.

Figure 1, left, also depicts the time response when the external layers oriented at 0° are replaced with optimised layers having the stiffness distributions of Figure 2 (corresponding to the variable orientation
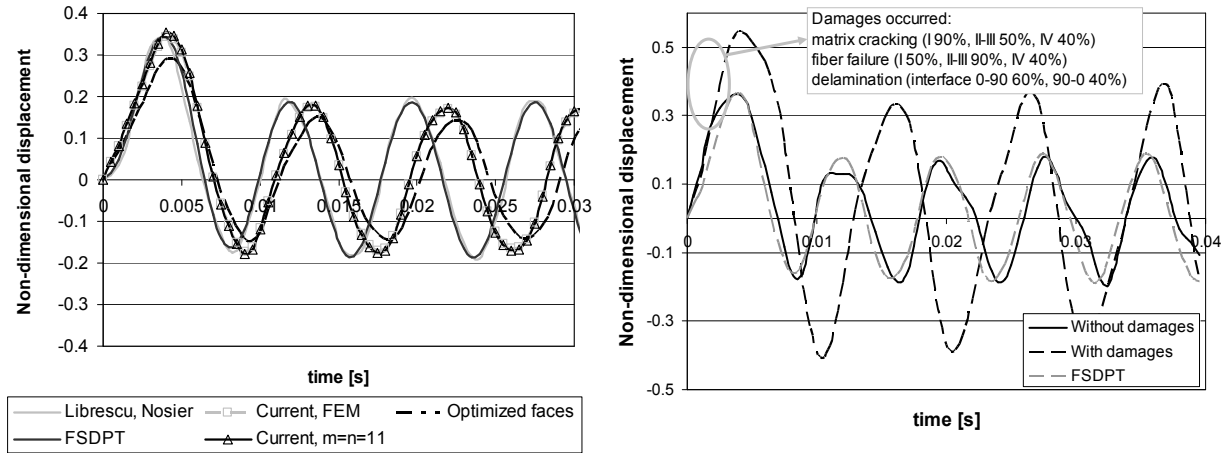
**Figure 1.** Triangular blast pulse loading: nondimensional deflection time history for a [0/90/90/0] laminate.
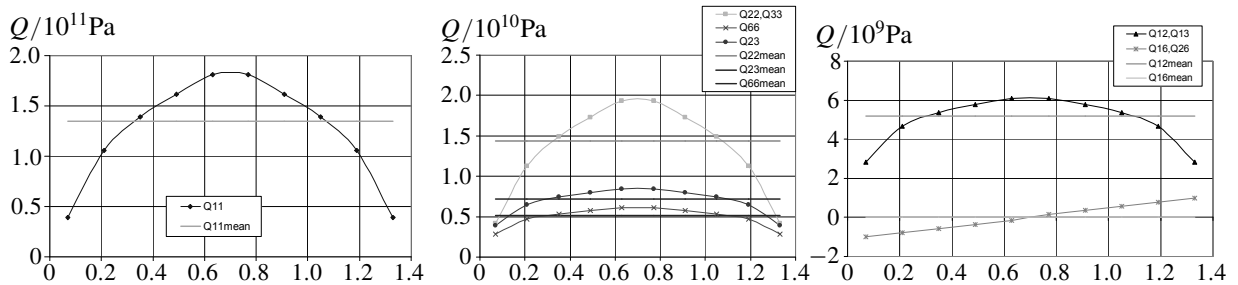


**Figure 2.** Stiffness distribution for the optimised layers. The horizontal coordinate is the in-plane direction $x$, in meters.

of reinforcement fibres presented in [Icardi and Ferrero 2008, Figure 3], here referred as OPT1). In this figure we regard the material as undamaged, although the hypothesis of mild loading is not consistent with the magnitude of the pressure pulse considered by Librescu and Nosier, the stresses being very large (that is, failure has already occurred at the loading level they consider). To be consistent with [Librescu and Nosier 1990], we will compare the stress fields without considering the degradation of the properties also in the remaining cases.

In Section 2.3 we analyse Figure 1, right, considering the effects of damage, and showing that at the first peak, after about 0.005 sec, the matrix damage is extended to 90% of first layer, 50% of second and third layers and 40% in the last layer. The area where the fibres have failed is 50% in the first layers, 90% in the subsequent two layers and 40% in the last layer. Delamination occurs at the 0°/90° and 90°/0° interfaces. In the first case, the delaminated area is 60% of the whole interface area, while in the last case it has an extension of 40%.

It appears by the comparison with the response predicted by the FSDPT model in Figure 1, left, that the high-order effects brought by the zigzag model have an increasing importance while the time unfolds. Also evident from the same figure is the beneficial effect of optimised layers in terms of motion amplitude
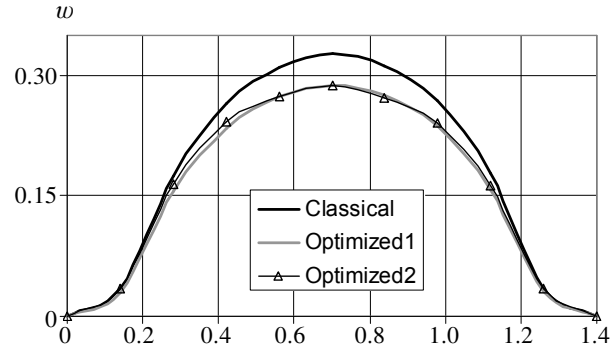
**Figure 3.** Transverse displacement (vertical axis, in meters) versus spanwise coordinate (horizontal axis, in meters) for the laminate with classical layers and the two laminates with optimised layers.
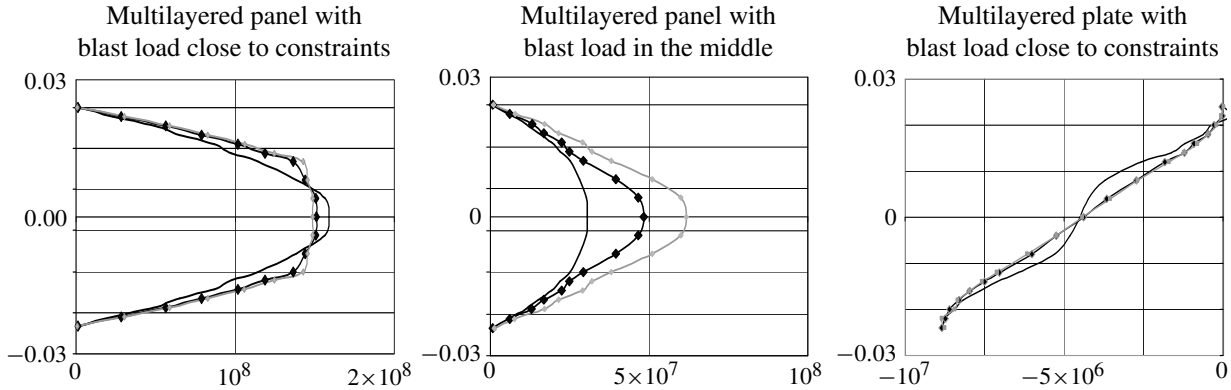


**Figure 4.** Normalized transversal shear stress (horizontal axis) versus thickness coordinate (vertical axis, in meters) for the laminate with classical layers (black curve with markers) and the two with optimised layers (smooth black curve = OPT1; grey curve = OPT2).

reduction (mean properties equal to those of the replaced layers). The effect on interlaminar stress fields of optimised layers is shown in Figure 4, which reports the stresses at the interfaces. A comparison is presented with the reference configuration and also with another optimised case having in plane shear stiffness with a maximum value close to the constraints and $Q_{16}$ and $Q_{26}$ with a double slope, here referred as OPT2.

These results are those corresponding to 3 msec after application of the pressure pulse. One can see in Figures 3 and 4 how the optimised layers that have limited deflections also can limit the magnitude of interlaminar stresses and oppose the spreading of the stress peaks at the inner interfaces. Application of the delamination criterion by Chang and Springer shows that the loading magnitude considered corresponds to a fully delaminated area at the first interface (starting from the bottom layer), as shown by the left column of Figure 5, while at the next interfaces the central region remain undamaged. When an optimised layer OPT2 is incorporated, these regions enlarge to the whole plate and at the first interface there is a central region where delamination does not take place; see middle column of Figure 5. Thus, it appears
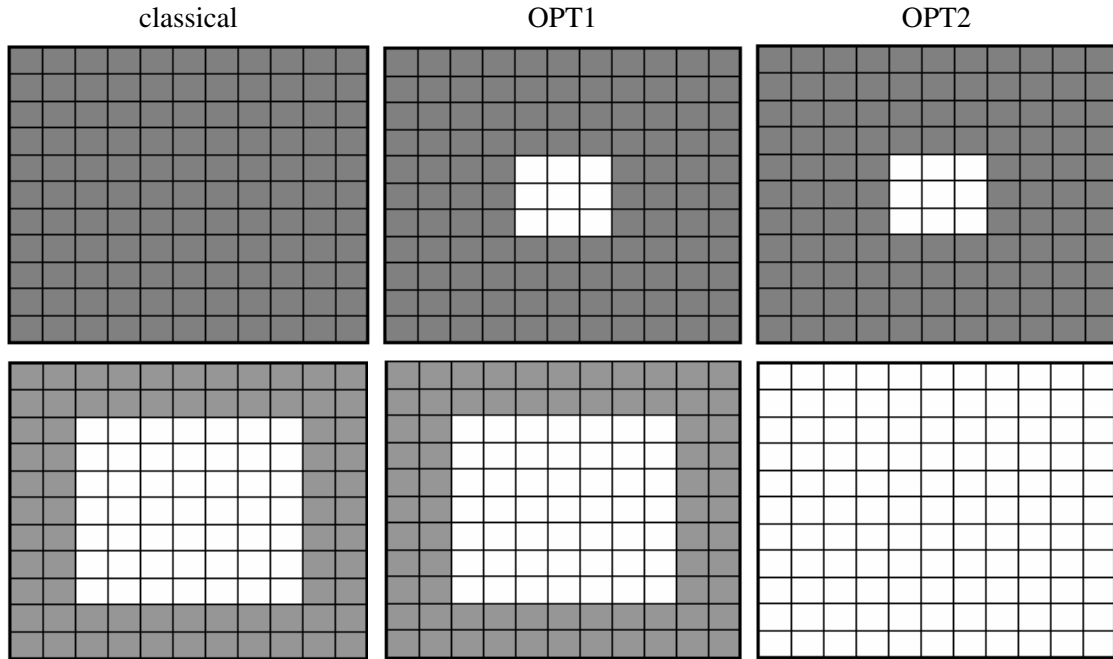
classical          OPT1          OPT2



**Figure 5.** Delaminated area (shown in grey) at the first interface (0/90, top row) and at the third (90/0, bottom row). Left column, classical laminate; middle column, OPT1; right column, OPT2.

that the present optimisation technique can both improve the response and the strength. Obviously, orienting the reinforcement fibres in a complementary way, the opposite result could be found.

**5.2. *Sandwich plates.*** Now consider cases of sandwich panels subjected to different blast pulse loading, with the purpose to assess the accuracy of the structural model when it predicts their transient motions and discuss the implications of the optimisation. Cases with optimised face sheets, i.e. incorporating optimised layers with the features discussed above, and with or without an optimised distribution of the core properties across the thickness will be considered. The reference configurations are chosen among the sample cases presented in [Hause and Librescu 2005, Figure 7 and 12].

The first of these refers to a pulse step of 0.005 sec, using the same $10 \times 10$ in-plane discretization than in the former case. The time response for this case as predicted by Hause and Librescu, by the present structural finite element model with energy updating, by the CLPT and FSDPT models using the Galerkin method (with only one term in both directions) and by the present model varying the core properties across the thickness is represented in Figure 6. The stacking sequence for this case is $[45/-45/45/-45/45/\text{core}/45/-45/45/-45/45]$; the length-to-thickness ratio is 20.97. It appears again that the high-order effects incorporated in the current model results in little larger deflections, while frequencies remain unchanged. This result is consequent to the large deformation in the transverse direction and to the very high bending stiffness peculiar of sandwich panels. The four core configurations considered produce a different response, but the variation is not large. All have the same mean properties that correspond to those of the reference case and all produce a reduction in the amplitude of motions. The
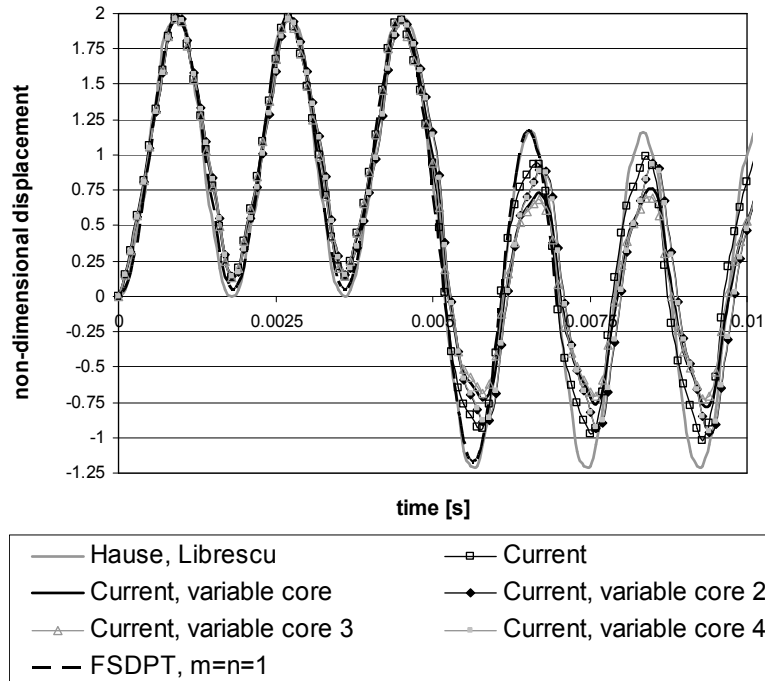
**Figure 6.** Step blast pulse loading: non-dimensional deflection time history for the sandwich plates with [45/−45/45/−45/45/core/45/−45/45/−45/45] lay-up.

first case OPT-S1 corresponds to a *V* variation of the core properties across the thickness increasing at the midplane; it represents a simplified suboptimal variation that simulates in a rough way the optimised variation of (21)–(23), here referred to as OPT-S2 (where the property variation on the thickness has an hyperbolic shape. The case OPT-S3 is similar to OPT-S1 but has properties that decrease from the interfaces with the face sheets to the midplane. The last case OPT-S4 is similar to OPT-S2, but has the minimum value at the midplane.

Consider now the sample case treated in [Hause and Librescu 2005, Figure 12] with the purpose to show the high sensitivity of the response to the lay-up variation of the faces, for a sonic boom pressure pulse. The lay-up considered in by House and Librescu was $(t/-t/t/-t/t/\text{core}/t/-t/t/-t/t)$, with $t$ respectively equal to $45°$, $30°$, $0°$. The response predicted by the present model for these three cases is reported in Figure 7. It appears that also for this sample case, the FSDPT model and the Galerkin's solution with just one term in both the directions $x$ and $y$ is equivalent to that of Hause and Librescu, as shown by the results for $t = 0°$ and $t = 45°$. A similar result, not shown in the figure for readability, was also obtained for $t = 30°$.

The effect of incorporation of cores with variable properties across the thickness is shown in Figure 8. The sample cases considered in this figure pertains to the case $t = 0°$ and the core variations OPT-S2 and OPT-S3. Besides the beneficial effect of the core property variation across the thickness that is shown by both the configurations considered, it has to be noted that a different behaviour is presented for different boundary conditions. Numerical tests show that for pinned edges better results are obtained in terms
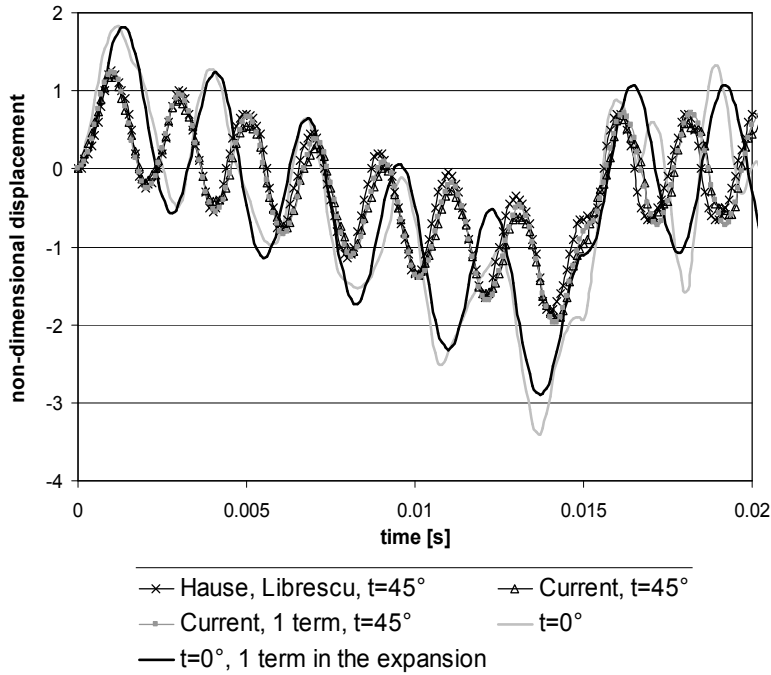
**Figure 7.** Sonic boom blast pulse loading: nondimensional deflection time history for sandwich plates with $[t/-t/t/-t/t/\text{core}/t/-t/t/-t/t]$ lay-up.
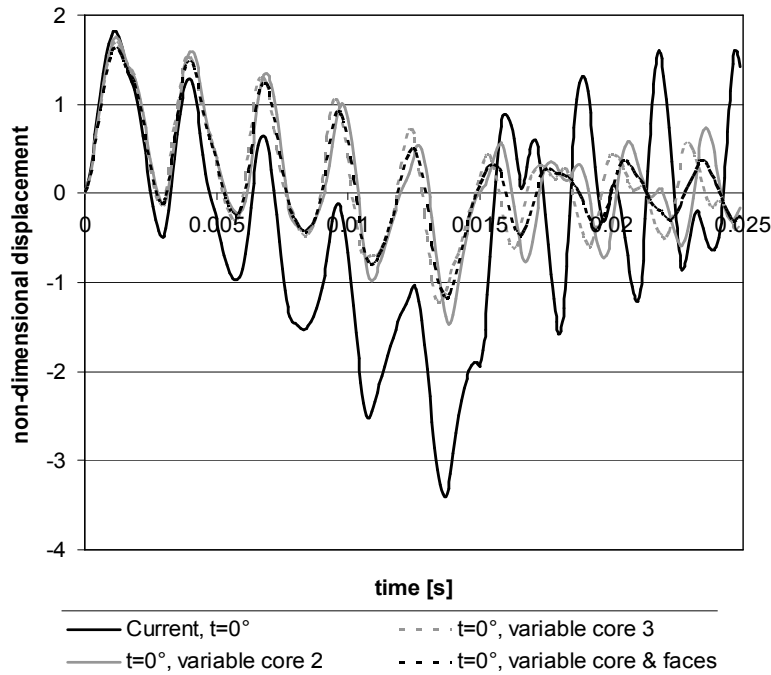


**Figure 8.** Sonic boom blast pulse loading: nondimensional deflection time history for optimised sandwich plates.

of vibrations suppression when the elastic coefficients of the core are decreasing from the face sheets interfaces to the midplane, as in OPT-S3, while the opposite occurs for simply supported edges: OPT-S2 is more efficient.

To assess whether the incorporation of optimised faces in sandwich panels with optimised core can consistently decrease the amplitude of motions, the sample case of a sandwich panel with core of type OPT-S2 (i.e., not the most efficient case) and faces with a [0/90/90/0] lay-up was considered. To be self-contained, the motions for this case are not reported; it is just reported that if the 0° layers are substituted with optimised layers, as described in Section 5.1, a reduction of the amplitude to 1/6 is obtained already in the first instants of motion with respect to the reference case with constant properties of the 0° layers (equivalent to the mean value of optimised layers) and this ratio is kept while the time unfolds.

The interlaminar stress fields for the case $t = 0°$ and cores with variable properties OPT-S2 and OPT-S3 are reported in Figure 9, which refers to 0.11 sec after application of the pressure pulse. Their magnitude being large, the pressure pulse considered in [Hause and Librescu 2005] for this sample case does not reflect the hypothesis of mild loading, therefore failures occurred during the motions that also in the present paper have not been considered. Just comparing the stress fields without considering the degradation of properties, it appears that the variable core properties reduce the critical stress concentration of shear stresses at the interface with the core and spread these stresses across the core. Beneficial effects are seen also for the transverse normal stress, since in the region close to the lower interface where they are peeling, i.e., tensile, the magnitude consistently decreases, and they also decrease at the upper interface where they are compressive; since they are spread across the core. This reduction of the critical interfacial concentration by spreading the stresses was also the objective pursued by the former studies on functionally graded materials. While in such studies the core property variation was postulated, in the present paper it is grounded on energy considerations and still appears successful.

Applying the Chang–Springer criterion for delamination it appears that in the reference case the upper interface with the core is fully delaminated, while the lower one is undamaged, as shown by Figure 10. The situation is different in the optimised cases; for example in the case OPT-S1 some regions are
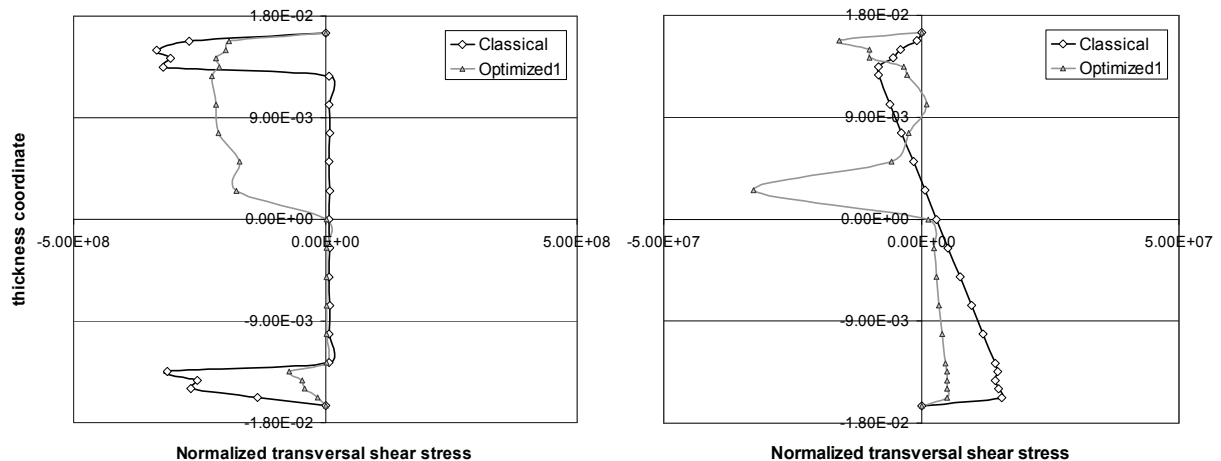


**Figure 9.** Transverse shear (left) and normal (right) stresses across the thickness for the sandwich plate with classical and optimised configuration.
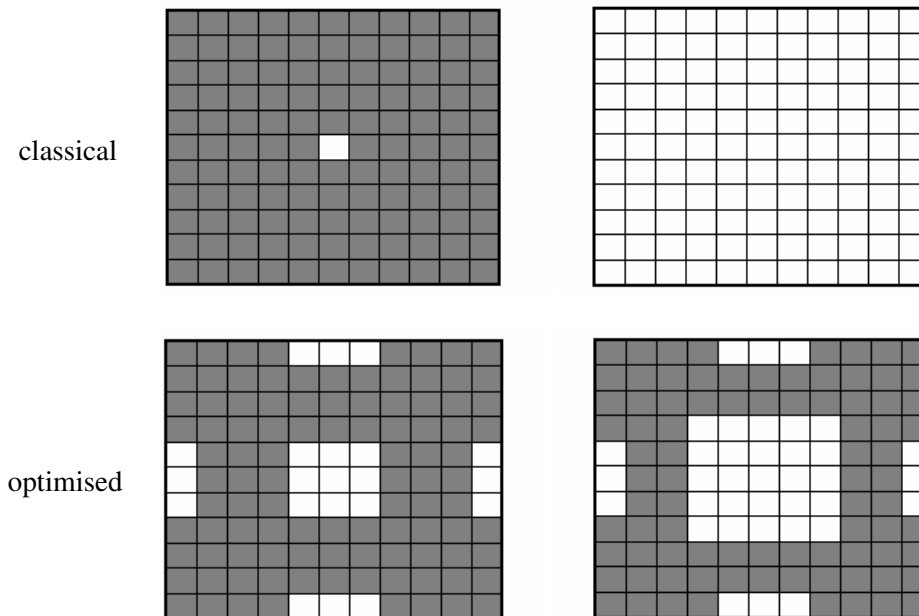
**Figure 10.** Delaminated area (shown in grey) at the two core-face interfaces for the sandwich plate with classical (top row) and optimised (bottom row) configurations.

preserved from delamination at the upper interface, while the lower interface present a delamination damage distributed in a similar way because the stress peak are spread across the thickness. This means that all the constituent materials contribute to the absorption of the incoming energy due to the pulse pressure, with evident practical advantages.

## Concluding remarks

The dynamic response and the stress fields of laminated and sandwich flat panels undergoing impulsive pressure loading have been investigated for different pulse pressure time histories. A refined zigzag model with a piecewise high-order variation of in-plane and transverse displacements is employed as structural model, which is incorporated through a strain energy updating into a conventional shear deformable plate element. The reason is that the direct implementation of the zigzag model involves displacement derivatives as nodal DOFs, which makes the elements inefficient from the computational viewpoint. The current model represents a good compromise because it requires a lower computational effort than discrete-layer models for providing a lower, but still rather good accuracy of predictions.

A recently developed technique is employed for relaxing the critical interlaminar stress concentrations at the interfaces of constituent layers. With this technique, the optimal through-the-thickness distribution of the core properties and the in-plane distribution of the stiffness properties of the face sheets (and of the constituent layers of laminates) are found maximising the strain energy absorbed through membrane and bending modes and minimizing that absorbed by out-of-plane modes involving the interlaminar stresses. While in the former studies on functionally graded materials the core property variation was postulated, in the present paper it results from energy considerations.

It appears that the current technique reduces the critical interlaminar stress concentrations (that is, it spreads them across the thickness), with beneficial effects on the strength at the onset of damage. It also improves the dynamic response, since it limits deflections while time unfolds. Even simple suboptimal distributions that approximate in a rough way the optimised variation of stiffness properties appear effective in the numerical applications.

## References

[Apetre et al. 2006] N. A. Apetre, B. V. Sankar, and D. R. Ambur, "Low-velocity impact response of sandwich beams with functionally graded core", *Int. J. Solids Struct.* **43**:9 (2006), 2479–2496.

[Birman and Bert 1987] V. Birman and C. W. Bert, "Behaviour of laminated plates subjected to conventional blast", *Int. J. Impact Eng.* **63**:3 (1987), 145–155.

[CAA 2001] "Aircraft hardening research programme: final overview report", CAA Paper 2001/9, Civil Aviation Authority, London, 2001, Available at http://www.caa.co.uk/docs/33/CAPAP200109.PDF.

[Cederbaum et al. 1988] G. Cederbaum, L. Librescu, and I. Elishakoff, "Random vibration of laminated plates modeled within a high-order shear deformation theory", *J. Acoust. Soc. Am.* **84**:2 (1988), 660–666.

[Cederbaum et al. 1989] G. Cederbaum, L. Librescu, and I. Elishakoff, "Response of laminated plates to non-stationary random excitation", *Struct. Safety* **6**:2–4 (1989), 99–113.

[Cheng and Benveniste 1968] D. H. Cheng and J. E. Benveniste, "Sonic boom effects on structures: a simplified approach", *Trans. New York Acad. Sci., Ser. II* **30** (1968), 457–478.

[Crocker and Hudson 1969] M. J. Crocker and R. R. Hudson, "Structural response to sonic booms", *J. Sound Vib.* **9**:3 (1969), 454–468.

[Dobyns 1981] A. L. Dobyns, "Analysis of simply-supported orthotropic plates subjected to static and dynamic loads", *AIAA J.* **19**:5 (1981), 642–650.

[Gupta 1985] A. D. Gupta, "Dynamic analysis of a flat plate subjected to an explosive blast", pp. 491–496 in *Computers in engineering, 1985: proceedings of the 1985 ASME International Computers in Engineering Conference and Exhibition* (Boston, 1985), vol. 1, edited by R. Raghavan and S. M. Rohde, ASME, New York, 1985.

[Gupta et al. 1986] A. D. Gupta, F. H. Gregory, and R. L. Bitting, "Dynamic response of a simply-supported rectangular plate to an explosive blast", pp. 385–390 in *SECTAM XIII proceedings: the Southeastern Conference on Theoretical and Applied Mechanics* (Columbia, SC, 1986), vol. 1, edited by W. F. Ranson and J. H. Biedenbach, College of Engineering, University of South Carolina, Columbia, SC, 1986.

[Hause and Librescu 2005] T. Hause and L. Librescu, "Dynamic response of anisotropic sandwich flat panels to explosive pressure pulses", *Int. J. Impact Eng.* **31**:5 (2005), 607–628.

[Hause and Librescu 2007] T. Hause and L. Librescu, "Dynamic response of doubly-curved anisotropic sandwich panels impacted by blast loadings", *Int. J. Solids Struct.* **44**:20 (2007), 6678–6700.

[Hayman 1996] B. Hayman, "Underwater explosion loadings on foam-cored sandwich panels", in *Sandwich construction 3: proceedings of the Third International Conference on Sandwich Construction* (Southampton, 1995), vol. 2, edited by H. G. Allen, Engineering Materials Advisory Service, Cradley Heath, 1996.

[Houlston et al. 1985] R. Houlston, J. E. Slater, N. Pegg, and C. G. DesRochers, "On analysis of structural response of ship panels subjected to air blast loading", *Comput. Struct.* **21**:1–2 (1985), 273–289.

[Icardi 2001] U. Icardi, "Higher-order zig-zag model for analysis of thick composite beams with inclusion of transverse normal stress and sublaminates approximations", *Compos. B Eng.* **32**:4 (2001), 343–354.

[Icardi 2007] U. Icardi, "$C^\circ$ plate element based on strain energy updating and spline interpolation, for analysis of impact damage in laminated composites", *Int. J. Impact Eng.* **34**:11 (2007), 1835–1868.

[Icardi and Ferrero 2008] U. Icardi and L. Ferrero, "A new tailoring optimization approach for improving structural response and energy absorption capability of laminated and sandwich composites", *J. Mech. Mater. Struct.* **3**:4 (2008), 729–760.

[Icardi and Ferrero 2009] U. Icardi and L. Ferrero, "Impact analysis of sandwich composites based on a refined plate element with strain energy updating", *Compos. Struct.* **89**:1 (2009), 35–51.

[Jiang and Olson 1994] J. Jiang and M. D. Olson, "Modelling of underwater shock-induced response of thin plate structures", Technical Report 39, Department of Civil Engineering, University of British Columbia, Vancouver, 1994.

[Kim and Han 2006] D.-K. Kim and J.-H. Han, "Establishment of gun blast wave model and structural analysis for blast load", *J. Aircraft* **43**:4 (2006), 1159–1168.

[Langdon and Schleyer 2006] G. S. Langdon and G. K. Schleyer, "Deformation and failure of profiled stainless steel blast wall panels, III: Finite element simulations and overall summary", *Int. J. Impact Eng.* **32**:6 (2006), 988–1012.

[Librescu and Na 1998] L. Librescu and S. Na, "Dynamic response of cantilevered thin-walled beams to blast and sonic-boom loadings", *Shock Vib.* **5**:1 (1998), 23–33.

[Librescu and Nosier 1990] L. Librescu and A. Nosier, "Response of laminated composite flat panels to sonic boom and explosive blast loadings", *AIAA J.* **28**:2 (1990), 345–352.

[Librescu et al. 2004] L. Librescu, S.-Y. Oh, and J. Hohe, "Linear and non-linear dynamic response of sandwich panels to blast loading", *Compos. B Eng.* **35**:6–8 (2004), 673–683.

[Librescu et al. 2005] L. Librescu, S. Na, P. Marzocca, C. Chung, and M. K. Kwak, "Active aeroelastic control of 2-D wing-flap systems operating in an incompressible flowfield and impacted by a blast pulse", *J. Sound Vib.* **283**:3–5 (2005), 685–706.

[Librescu et al. 2006] L. Librescu, S.-Y. Oh, and J. Hohe, "Dynamic response of anisotropic sandwich flat panels to underwater and in-air explosions", *Int. J. Solids Struct.* **43**:13 (2006), 3794–3816.

[Makinen 1999] K. Makinen, "Underwater shock loaded sandwich structures", Report 99-01, Department of Aeronautics, Royal Institute of Technology, Stockholm, 1999.

[Proctor 1972] J. F. Proctor, "Internal blast damage mechanisms computer program", Technical Report NOLTR 72-231, Naval Ordnance Laboratory, Silver Spring, MD, 1972.

[Rajamani and Prabhakaran 1980] A. Rajamani and R. Prabhakaran, "Response of composite plates to blast loading", *Exp. Mech.* **20**:7 (1980), 245–250.

[Rudrapatna et al. 2000] N. S. Rudrapatna, R. Vaziri, and M. D. Olson, "Deformation and failure of blast-loaded stiffened plates", *Int. J. Impact Eng.* **24**:5 (2000), 457–474.

[Shin and Geers 1994] Y. S. Shin and T. L. Geers, *Response of marine structures to underwater explosions*, Shock and Vibration Research, Monterey, CA, 1994.

[Simmons and Schleyer 2006] M. C. Simmons and G. K. Schleyer, "Pulse pressure loading of aircraft structural panels", *Thin-Walled Struct.* **44**:5 (2006), 496–506.

[Song et al. 1998] O. Song, J.-S. Ju, and L. Librescu, "Dynamic response of anisotropic thin-walled beams to blast and harmonically oscillating loads", *Int. J. Impact Eng.* **21**:8 (1998), 663–682.

[Xue and Hutchinson 2004] Z. Xue and J. W. Hutchinson, "A comparative study of impulse-resistant metal sandwich plates", *Int. J. Impact Eng.* **30**:10 (2004), 1283–1305.

[Zhu 1996] L. Zhu, "Transient deformation modes of square plates subjected to explosive loadings", *Int. J. Solids Struct.* **33**:3 (1996), 301–314.

UGO ICARDI: ugo.icardi@polito.it
*Dipartimento di Ingegneria Aeronautica e Spaziale, Politecnico di Torino, Corso Duce degli Abruzzi 24, 10129 Torino, Italy*

LAURA FERRERO: laura.ferrero@polito.it
*Dipartimento di Ingegneria Aeronautica e Spaziale, Politecnico di Torino, Corso Duce degli Abruzzi 24, 10129 Torino, Italy*